Molecular Electronics with Endohedral Metallofullerenes: The Test Case of $La_2@C_{80}$ Nanojunctions

Ángel J. Pérez-Jiménez*

Departamento de Química-Física, Universidad de Alicante, E-03080, Alicante, Spain

Received: August 1, 2007; In Final Form: September 19, 2007

Controlling the positions of the encapsulated atoms in endohedral metallofullerenes may help in designing functional devices for molecular electronics. Ab initio calculations performed here show that both the positions of the La atoms and the electronic transport through $La_2@C_{80}$−metal nanojunctions are largely influenced by the metallic leads, which act both as chemical and as transport functionalizers of the molecule. The calculations also indicate that the transport properties for this kind of molecular nanobridge can be modulated by the total charge present in the nanodevice, especially for tip−molecule−tip or surface−molecule−tip nanostructures.

1. Introduction

Molecular electronics aims at using just one or a few molecules to perform the basic functions of digital electronics in order to meet the ever-increasing needs for speed and efficiency at reasonable costs demanded by information technologies.[1−3] Examples of molecular wires, diodes, switches, and storage elements have already been proposed to do the corresponding transmission, processing, manipulation, and storage operations.[3−5] Endohedral metallofullerenes (EMs) are, in principle, interesting candidates for fabricating useful molecular electronics devices because they combine fullerene-like with metallic properties.[6] Actually, it has been observed recently that EM thin films act as field-effect transistors,[7] although their transport properties as single molecules remain unexplored. The fact that the metal atoms inside the fullerene cage of some EMs are rather free to move at room temperature,[8−10] and that they are positively charged,[11,12] suggests that EMs could be used in molecular nanodevices if the movement of the La atoms could be restricted, taking advantage of their charged nature, as suggested by theoretical calculations.[13] This kind of control has recently been achieved experimentally by exohedral chemical functionalization with an electron-donating molecule on the outer surface of the [80]fullerene cage in $La_2@C_{80}$ and $Ce_2@C_{80}$.[14,15] A further step in the above direction is taken here, where ab initio calculations show that the rather free movement of the La atoms in $La_2@C_{80}$ can be hindered by just placing the molecule between two metal electrodes, which act as a couple of exohedral functionalizers that are also key for the electronic transport properties of the nanojunction. It will be shown that this can be used to design useful EM-based nanodevices.

2. Computational Details

2.1. Potential Energy Curves. The potential energy curves (PECs) shown in this work have been calculated with the Gaussian03 package[16] at intervals of 0.25 Å for the metal−molecule distance using the Kohn−Sham Density Functional Theory[17,18] (DFT) with the B3LYP exchange-correlation functional.[19,20] The basis sets and pseudopotentials used are the following: the all-electron Dunning−Huzinaga full double-ζ basis set for C,[21] the Hay−Wadt pseudopotential and double-ζ basis set for La,[22] and the Christiansen and co-workers pseudopotential and minimal basis set for Au and Al.[23] The corresponding contractions are (9s5p)/[3s2p], (5s5p3d)/[3s2p2d], (3s3p4d)/[1s1p1d], and (4s4p)/[1s1p] for C, La, Au, and Al, respectively. To reduce the computational cost, only the gold−molecule distance has been varied, while the molecular and metal geometries, as well as the relative orientation between each other, have been kept fixed in the calculations. The molecular geometries correspond to DFT-optimized structures of isolated $La_2@C_{80}$ molecules with D_{3d} and D_{2h} symmetry. The binding energy is calculated by subtracting the energy of the separated metal structures and molecule to that of the metal−molecule cluster at the minimum of the PEC.

2.2. Transport Calculations. The conductance and current−voltage profiles have been calculated with the ALACANT[24] code, interfaced with the Gaussian03 package. ALACANT implements self-consistent non-equilibrium Green's function (NEGF) techniques[25] at the DFT level to evaluate the current of a nanojunction from first principles.[26−29] More precisely, the conductance at zero bias is calculated by means of Landauer's formula[25]

$$G = G_0 T = \frac{2e^2}{h} T \tag{1}$$

that relates the conductance G with the transmission probability T for electrons to go from one electrode to the other, the proportionality constant, G_0, being the so-called conductance quantum. The transmission probability can be calculated from

$$T(E) = \mathrm{Tr}[\Gamma_L(E)\mathbf{G}^{(+)}(E)\Gamma_R(E)\mathbf{G}^{(-)}(E)] \tag{2}$$

where the system Green's function matrices are evaluated from

$$\mathbf{G}^{(\pm)} = [(E \pm i\delta)\mathbf{S} - \mathbf{F} - \Sigma^{(\pm)}(E)]^{-1} \tag{3}$$

by dividing the whole (infinite) system in two parts: a (finite) cluster region comprising the molecule and a small portion of the metal electrodes with Fock (**F**) and overlap matrices (**S**) defined over the corresponding atomic basis set of the cluster, and two semi-infinite (L for left and R for right) regions that

* E-mail: aj.perez@ua.es.

10.1021/jp076143q CCC: $37.00
Published on Web 11/07/2007

contribute through the corresponding self-energy matrices: $\Sigma^{(\pm)} = \Sigma_L^{(\pm)} + \Sigma_R^{(\pm)}$. These are evaluated with a parametrized tight-binding Bethe lattice model with the coordination number and effective parameters appropriate for the type of electrodes. $\Gamma_{L,R}$ can be obtained from the latter by using the following relationship

$$\Gamma_{L,R} = i[\Sigma_{L,R}^{(+)} - \Sigma_{L,R}^{(-)}] \quad (4)$$

To guarantee the correct coupling between the two parts (cluster + semi-infinite regions), we performed a self-consistent process that uses the density matrix obtained at one cycle

$$\mathbf{P} = -\frac{2}{\pi}\int_{-\infty}^{E_F} \mathrm{Im}[\mathbf{G}^{(+)}(E)]\mathrm{d}E \quad (5)$$

to re-evaluate **F** and, from this, $\mathbf{G}^{(\pm)}$ at the next one until the modification in **P** is appropriately small. The value of the Fermi energy, E_F, is determined by fixing the total number of electrons in the cluster, given by

$$\mathrm{Tr}[\mathbf{PS}] + q \quad (6)$$

to a prescribed value, with $Q = -q$ being the excess charge imposed on it.

For finite bias, the current I is evaluated from

$$I = \frac{2e}{h}\int_{-V_b/2}^{+V_b/2} T(E, V_b)\mathrm{d}E \quad (7)$$

at bias steps of 0.2 V between 0 and 2 V. In the above expression, $T(E, V_b)$ denotes the transmission probability at a given energy and bias voltage. It is also evaluated from eqs 2 and 3, but in the self-consistent process the out-of-equilibrium density matrix must be evaluated from

$$\mathbf{P} = -\frac{i}{\pi}\int_{-\infty}^{+\infty} [\mathbf{S}^{-1}\mathbf{G}^{<}(E)\mathbf{S}^{-1}]\mathrm{d}E \quad (8)$$

where the so-called *lesser* Green's function matrix is given by

$$\mathbf{G}^{<}(E) = i\mathbf{G}^{(-)}(E)[\, f_L(E)\, \Gamma_L(E) + f_R(E)\, \Gamma_R(E)]\mathbf{G}^{(+)}(E) \quad (9)$$

where f_L and f_R are the Fermi distribution functions on the left and right electrodes, respectively. The interested reader may find further details on the implementation of the method in refs 26−29.

3. Results and Discussion

It is well known that the transport properties of a molecular nanodevice depend on the interrelationship between its spatial and electronic structures, which are the subjects of the next two sections.

3.1. Metallic Leads Hinder the Movement of the La Atoms in $La_2@C_{80}$−Gold Nanobridges. As mentioned already in the previous section, the geometry of the $La_2@C_{80}$−metal nanobridges is analyzed here by means of DFT calculations. However, the "large" size of the corresponding clusters prevents a complete DFT study of all of the structures that may be present in the formation of the nanojunction. For this reason, a small but representative number of structures have been considered, which are described next.

We start by noting that, for an isolated $La_2@C_{80}$ molecule, both La atoms move between 10 *equivalent* D_{3d} configurations through intervening D_{2h} configurations placed a few kcal/mol above the former.[10,30,31] In each of these 10 D_{3d} configurations, both La atoms are simultaneously located below one of the 20 carbon atoms joining three hexagons of the [80]fullerene cage, while in the D_{2h} configurations they are aligned with C_2 axes passing through six-membered carbon rings. A question arises as to which extent the aforementioned movement of the La atoms is influenced by the presence of the metallic leads when the nanobridge forms and how stable is the latter.

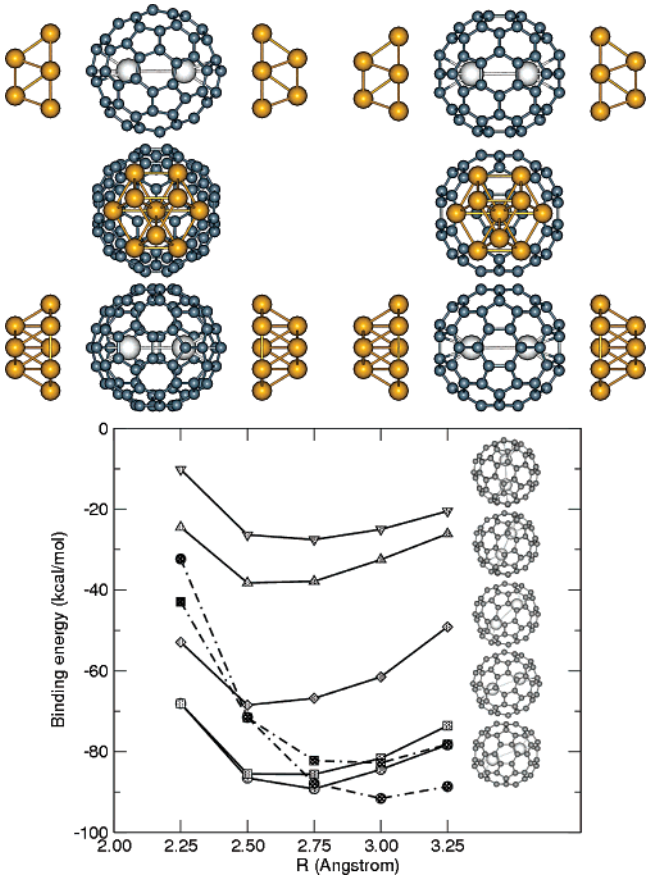

Figure 1. Top left: geometry of a cluster representing a $La_2@C_{80}$−gold nanojunction where the La atoms, and the C atoms under which the former are placed, are aligned with both surface normals (atom-on-top structure); from top to bottom: side view, front view, top view. Top right: geometry of a cluster with the same relative orientation of the La atoms with respect to the gold surfaces, but with two hexagons facing them (hexagon-on-top structure); from top to bottom: side view, front view, top view. Bottom: potential energy curves for $La_2@C_{80}$−gold clusters representing nanojunctions with several orientations of the La atoms with respect to the metal surfaces for atom-on-top (solid lines, light shaded symbols) and hexagon-on-top (dotted-dashed lines, dark shaded symbols) structures. *R* represents the distance between the nearest carbon (hexagon face) to the gold surface for the atom-on-top (hexagon-on-top) structure. The side view of each structure (the gold atoms have been removed for simpicity) are depicted at the right of each curve, except for the two most stable ones, which correspond to those depicted above with both La atoms being nearest to each surface. The first three geometries, from top to bottom, correspond to atom-on-top structures where the La−La segment is oriented at 90° (triangles down), 71° (triangles up), and 66° (diamonds) with respect to the surface normal. The last two geometries correspond to a 21° orientation of the La−La segment for the atom-on-top (light shaded squares) and the hexagon-on-top (dark shaded squares) structures, respectively.

The answer can be found after inspecting Figure 1, where it is clearly seen that the presence of the metal surfaces at each side of the molecule in the nanojunction breaks the degeneracy of the D_{3d} molecular configurations depending on the relative orientation between the La atoms and the metal contacts. The top-left panel of this figure depicts a $La_2@C_{80}$−gold nanobridge (hereafter termed atom-on-top) structure where the [80]fullerene

cage is oriented with two of the above-mentioned 20 carbon atoms facing each a gold surface modeled by a two-slab structure of 10 gold atoms representing the (111) surface of an fcc crystal with a lattice constant of 4.0786 Å. For this relative orientation between the fullerene cage and the electrodes, the 20 carbons mentioned above can be grouped in *three* sets leading to three groups of isoenergetic D_{3d} molecular configurations that differ in the relative orientation between the La atoms and the metal surfaces. This is illustrated by the corresponding PECs plotted in the bottom panel of Figure 1: light shaded circles, diamonds, and up triangle curves correspond to structures with angles of 0°, 66°, and 71° between the La−La segment and the surface normals, respectively. Two additional D_{2h} molecular configurations complete the study of the atom-on-top structure, where the relative orientation between the [80]fullerene cage and the metal surfaces is the same as in the three D_{3d} molecular configurations already commented on. In the first one (down diamonds), the two La atoms lie parallel to both surfaces while the second one (light-shaded squares) represents an intermediate configuration between the two most stable D_{3d} atom-on-top geometries. As mentioned above, this D_{2h} configuration would be a transition state between two equivalent D_{3d} configurations for an isolated $La_2@C_{80}$ molecule, but this is not the case once the molecule binds to the metallic electrodes. This results indicate that, the closer to both surfaces the La atoms are, the larger the stabilization found is, also breaking the role as a transition state of the D_{2h}-like configurations. The metal−molecule bond has an important electrostatic contribution; compare the amount of charge transferred to the metal surfaces derived from a Mulliken population analysis: 1.5, 1.3, 1.0, 0.5, and 0.0 electrons, with the binding energies: 89.2, 85.6, 68.5, 38.2, and 27.5 kcal mol^{-1}, corresponding to the minimum of each atom-on-top curve (solid lines, light-shaded symbols). We note also in passing that the metal−molecule interaction is quite strong, with the most stable structure having a binding energy of around 90 kcal mol^{-1}.

The electrostatic origin for this stabilization indicates that it must be similar for other orientations between the [80]fullerene cage and the metallic electrodes because it basically depends on the relative positioning of the La atoms with respect to the former. This is confirmed by additional PECs performed with a different orientation of the [80]fullerene cage, where now one of the hexagon rings is placed in front of each gold surface (hereafter termed hexagon-on-top structure), as illustrated in the top-right panel of Figure 1. Apart from the D_{2h} configuration where both La atoms are placed along the C_2 axis that coincides with the surface normals (dark shaded circles, dotted-dashed lines), an intermediate D_{3d}-like geometry (dark-shaded squares, dotted-dashed lines) with the La−La line tilted 21° with respect to the surface normal has been considered. Again, the most stable structure found is that with the two La atoms placed nearest to both metallic surfaces. The above results are in agreement with DFT calculations on $La_2@C_{80}(Si_2H_4(CH_2))_2$[13] and recent experimental evidence pointing at a restricted positioning of the La atom in $La@C_{82}$ molecules adsorbed on Cu(111) surfaces.[32] The latter is explained as the combined effect of electrostatic interactions and the restricted orientation of the adsorbed molecules with respect to the copper surface.[32] This seems to also be the case for the $La@C_{82}$−Au(111) nanobridges, although the fullerene cage seems to have some rotational freedom because the most stable atom-on-top and hexagon-on-top structures differ by just 2.4 kcal mol^{-1}. However, we will see in the next section that the orientation of the fullerene cage has little impact on the transport properties

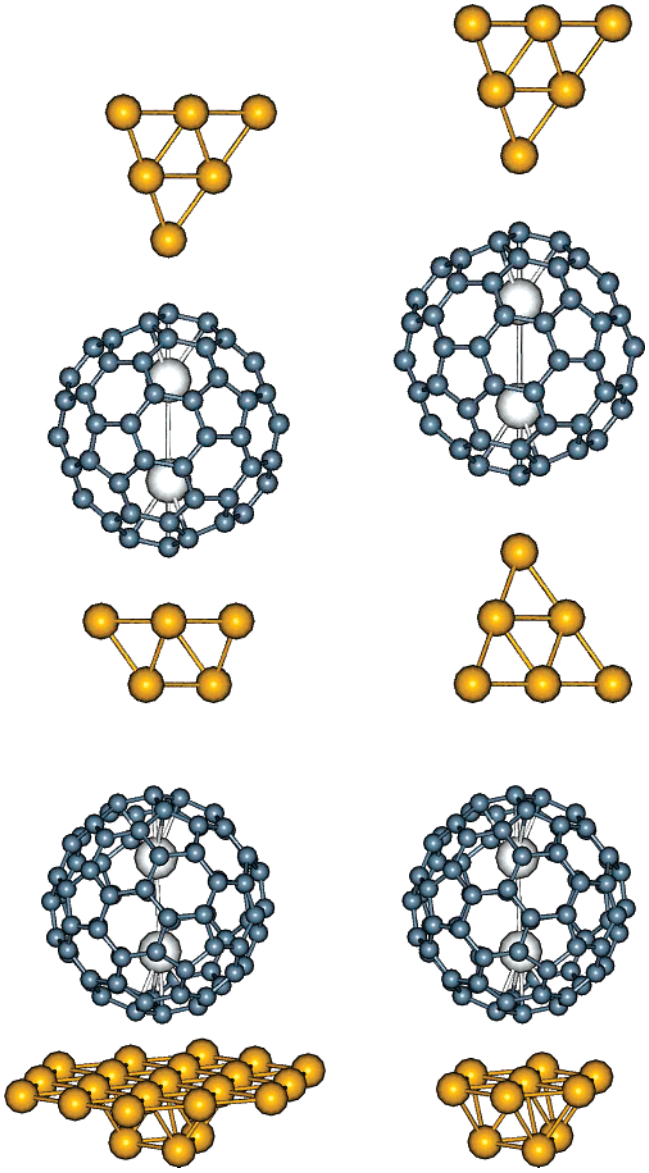

Figure 2. Geometries of additional clusters: tip−molecule−surface (top left), tip−molecule−tip (top right), molecule surface modeled by 22 atoms (bottom left) and molecule surface modeled by 10 atoms (bottom right).

of the molecular nanobridge. The data plotted in Figure 1 also suggest that the La atoms, despite having a clear preference to be oriented perpendicular to the metallic surfaces, have some chance to slightly change their orientation at room temperature to angles below 20°. This is also the case when the contact geometry changes from surface to tip, as indicated by additional calculations where just one (Figure 2, top left panel) or both (Figure 2, top right panel) surface models of the metal electrodes are substituted by 10-atom (111) tips for the atom-on-top structure at $R = 2.75$ Å. The lowest energy corresponds, again, to the cluster with the La−La segment lying parallel to the tip [111] direction, with binding energies of 84.3 and 78.6 kcal/mol for the surface−molecule−tip and tip−molecule−tip geometries, respectively. The next two most stable configurations also correspond to the same orientation between the Lanthanum atoms and the metal contacts already found for the surface−molecule−surface clusters (see Figure 1), with the D_{2h}-like and the next D_{3d} most stable configurations being, respectively, 3.8 and 20.7 kcal/mol above the ground state for the tip−molecule−surface clusters, while they are 2.7 and 17.0

kcal/mol less stable in the case of the tip−molecule−tip structures. Thus, the energy ordering of the relative lanthanum−metal contact position is independent of the actual contact geometry for the three kinds of clusters analyzed here: surface−molecule−surface, tip−molecule−surface and tip−molecule−tip.

Because the charge transfer between molecule and metal is important to both the binding and transport properties (see next section) of La@C_{82}−gold molecular nanodevices, additional calculations have been done enlarging the size of the metal part to 22 atoms, yet only one metal surface has been considered to keep the calculations computationally affordable: see Figure 2. The Mulliken charge transferred to the metal atoms is found to be 1.2 and 0.9 electrons for angles 0° and 71°, respectively, between the La−La segment and the surface normals, both calculated at a molecule−metal distance of $R = 2.75$ Å. Similar calculations with a 10-atom metal cluster (see also Figure 2) lead to 0.8 and 0.4 electrons transferred to the metal atoms. This results indicate that the *absolute* amount of charge transfer could be slightly larger than that reported above, but that the *relative* amount, which depends on the orientation of the La atoms, is correct giving further support to the relative ordering found for the structures analyzed. This will also not alter the main conclusions derived from the transport properties analyzed in the next section.

3.2. Electronic Transport is Dominated by a LUMO-Derived Resonance. It has been shown in the preceding section that the presence of gold surfaces restricts the internal motion of the La atoms, which prefer being simultaneously close to both surfaces. Now we explore the transport properties of La_2@C_{80}−metal nanojunctions for the most stable structures found previously. However, before commenting on the results obtained several technical issues are worth being mentioned. The DFT Fock matrix describing the cluster region is evaluated with the same combination of exchange-correlation functional, pseudopotentials, and basis sets used to obtain the PEC of the previous section. The cluster region used in the transport calculations involving metal surfaces comprises the La_2@C_{80} molecule (placed at the distance corresponding to the minimum energy of the PEC) and the 7 gold atoms in the first slab of the 10-atom surface model. The three atoms in the second slab have been removed from the cluster region in the transport calculations to lower the computational load. This limited description in the ab initio part of the electrodes could influence the results in two ways. First, the location of the minima in the PEC and the amount of charge transfer between molecule and electrode at the minimum could be markedly different between the one- and two-slab models for the electrodes. Therefore, additional PECs using the above seven atoms/one-slab model of the gold surfaces for the most and least stable structures of Figure 1 have been performed to check this. The results indicate that the distance at which the minimum of the PEC is located is not altered, with minor changes also in the amount of charge transfer: the overall Mulliken population for the gold atoms obtained for the one-slab PECs is 1.1 and −0.2 electrons for the most and least stable structures, respectively. These must be compared with the values 1.5 and 0.0 electrons of the two-slab model: the *difference* in charge between both structures is almost the same for the one-and two-slab models. The second issue is related to the appropriate size of the metal electrode that must be included in the cluster for a correct description of the out-of-equilibrium electrostatics when calculating the current. In the NEGF formalism, there is no need to solve Poisson's equation to account for this correctly, provided that a significant

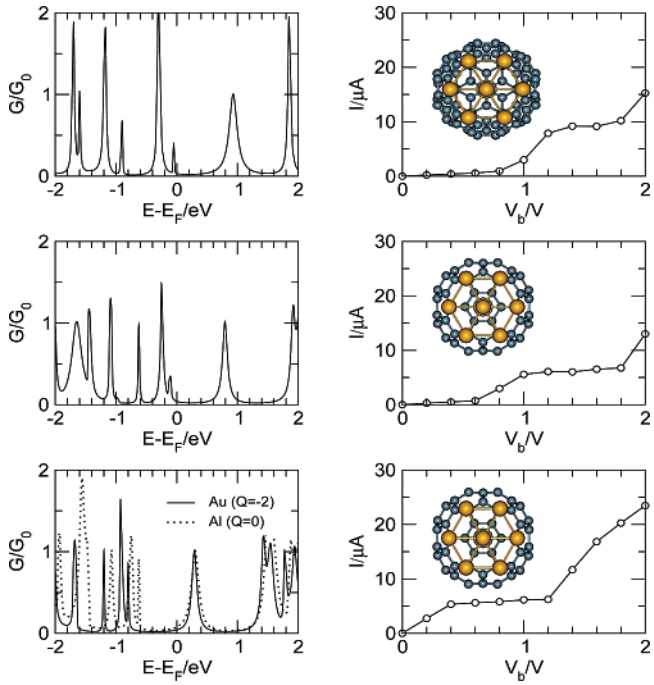

Figure 3. Electron transmission profiles (left) and corresponding *I*/*V* curves (right) of several La_2@C_{80}−gold nanojunctions whose geometry is depicted in the insets of the *I*/*V* plots. Top: atom-on-top structure. Middle: hexagon-on-top structure. Bottom: hexagon-on-top structure charged with an excess of two electrons (solid line); hexagon-on-top neutral structure with Al electrodes (dotted line).

part of the electrode has been included in the cluster, once the method achieves self-consistency by imposing overall charge neutrality.[28] However, computational limitations prevent a further study about the influence that the size of the metal leads included in the cluster region has on the *I*−*V* curves, but in any case it should affect each of the structures analyzed here in a similar way, thus being irrelevant for the differences found in their current−voltage characteristics. In summary, the actual positions of the resonance peaks with respect to the Fermi level could be slightly different than those reported in Figures 3 and 5, but this will not change the main conclusions derived from them.

The electron transmission profiles and *I*/*V* curves plotted in Figure 3 correspond to the atom-on-top (top panel) and hexagon-on-top (middle panel) structures. To better understand them, it is necessary for one to relate the resonances appearing at each side of the conductance gap around the Fermi level with the molecular orbitals they come from. The assignment can be unambiguously done by comparing the spatial form and the relative energies of molecular orbitals in the isolated molecule with transport channels of the nanojunction, both reported in Figure 4 for the most stable atom-on-top structure shown in Figure 1. The resemblance of the spatial form and the relative energies between orbitals and transport channels indicate that the leftmost (rightmost) peak in the conductance gap is a HOMO-derived (LUMO-derived) resonance. It is now easy to interpret the profiles plotted in Figure 3: the charge transferred from the molecule to the electrode places the Fermi level close to the HOMO-derived resonance. The extremely oriented form of the LUMO along the La−La segment explains the rather good interaction with the metal contacts, leading to a rather wide resonance with perfect transparency, 1 G_0, at its maximum. The positioning of the resonance peaks is almost the same for both atom-on-top and hexagon-on-top structures, yet the width is slightly lower in the latter, which is probably due to an overlap

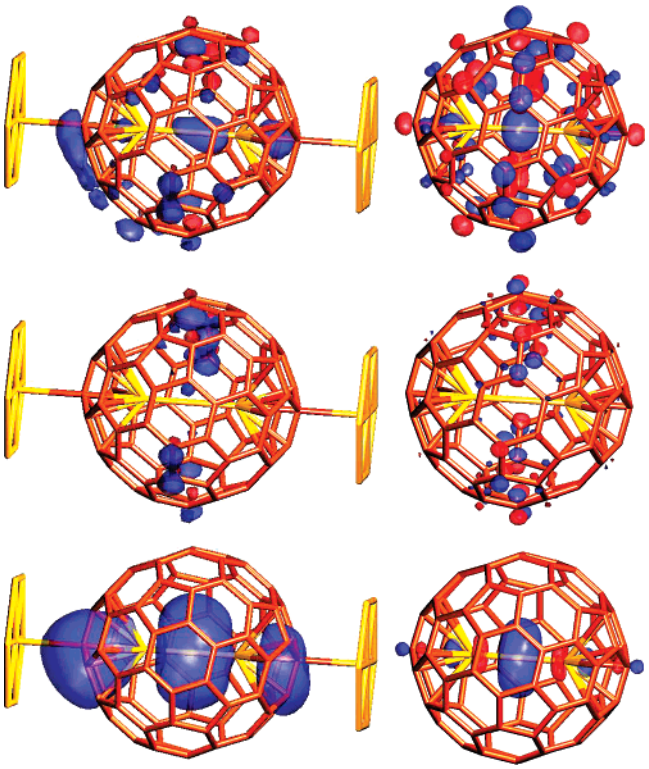

Figure 4. Left, from top to bottom: spatial form of the transport channels corresponding to the transmission peaks at −0.25, −0.05, and 0.95 eV with respect to the Fermi level shown in the top panel of Figure 3. Right, from top to bottom: spatial form of HOMO−1, HOMO, and LUMO orbitals of an isolated $La_2@C_{80}$ molecule (D_{3d} symmetry) with orbital energies of −0.2266, −0.2196, and −0.1728 Hartree, respectively.

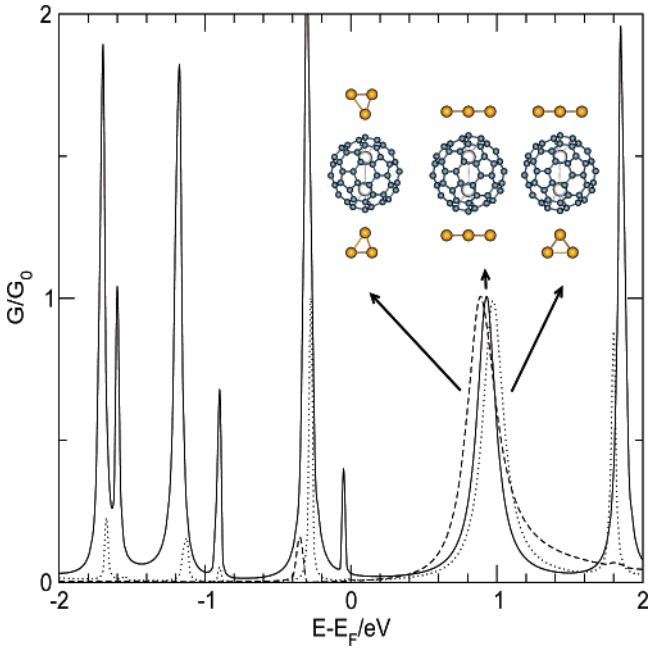

Figure 5. Electron transmission profiles of several atom-on-top $La_2@C_{80}$−gold nanojunctions differing in the structure of the metal contacts: surface−surface (solid line), surface−tip (dotted line), and tip−tip (dashed line). The pictures shown represent the cluster region used in the transport calculations. The metal−molecule distance has been fixed at 2.75 Å.

loss caused by an increase of 0.25 Å of the molecule−metal distance (see Figure 1). The calculated conductance gap for the structures, ∼1 eV, is in good agreement with experimental estimates for the HOMO−LUMO gap of $La_2@C_{80}$, ranging between 0.9 and 1.5 eV depending on the specific experimental techniques and conditions used.[33−35]

3.3. Field-Effect Transistors from $La_2@C_{80}$−Metal Nanobridges. As already mentioned in the Introduction, $La_2@C_{80}$ thin films have been reported to function as field-effect transistors,[7] a kind of function that their molecular electronic counterparts may also develop, as suggested by the bottom panel of Figure 3. This shows the conductance and *I*/*V* curves corresponding to the hexagon-on-top structure when the whole system is charged with an excess of two electrons (solid line), which mimics the result of using a gate electrode. We note in passing that the relation between the magnitude of the gate potential and the total charge accumulated in the nanobridge depends on the capacitance, which, in turn, depends on the whole molecular bridge−metallic gate setup. Without such information, it is not possible to relate the charge in the bridge with the gate potential needed to develop it and thus we are only considering here the *potential* use of this system as a field-effect transistor. Alternatively, the value of two electrons chosen for the excess charge is a reasonable one taken into account previous experimental work on molecular transistors.[36−38] It also leads to noticeable modifications of the transmission and current profiles: the charging process shifts the resonance peaks downward with respect to E_F, the *I*−*V* characteristics reflecting the corresponding changes in the electron transmission profiles, which qualitatively agree with the experimental results obtained for the thin film. The bottom-left panel of Figure 3 explores the changes on the conductance properties caused by using a more electropositive metal, aluminum, for the contacts. The electron transmission profile shown (dotted line) corresponds to the same hexagon-on-top structure used in the middle panel of the same figure. It is immediately apparent that the amount of charge transferred to the metal electrodes is much lower than that observed for gold, bringing the LUMO resonance much closer to the Fermi level. Furthermore, the change in the metal does not alter the good transmission properties of the LUMO-derived resonance, which still provides 1 G_0 conductance at its maximum peak.

The "on" to "off" conductance ratio for the two $La_2@C_{80}$−Au(111) nanobridges shown in Figure 3, calculated from the conductance at the Fermi level (off) and at the peak maximum (on), yields values of 31 and 24 for the atom-on-top and hexagon-on-top structures, respectively. This seemingly small value is caused by the relatively "high" conductance at the Fermi level: 0.032 G_0 and 0.041 G_0 for the atom-on-top and hexagon-on-top structures, respectively. This has been discussed previously by Lang[39] for the model case of the NaI molecule and is related to the long tails of the resonances involved. Inspired by Lang, a way to increase the on−off ratio for $La_2@C_{80}$−gold nanobridges is proposed here that takes advantage of the small overlap of the HOMO-derived resonance with the metal contacts (see Figure 4). This consists of changing the geometry of the metal contacts from surface to tip to reduce the HOMO−metal overlap even more. This, however, is a more realistic situation considering that the molecular nanobridges are usually constructed using scanning probes or breakjunction setups. The electron transmission profiles plotted in Figure 5 indicate that this is a step in the right direction: the conductance peaks for the HOMO and other resonances below it decrease dramatically when the surfaces are substituted by tips, increasing the "on" to "off" conductance ratio by an order of magnitude, now being ca. 130 for both the tip−molecule−tip and tip−molecule−surface geometries considered.

4. Conclusions

In this work, the potential use of endohedral fullerenes as the key component of molecular nanodevices has been addressed. The ab initio calculations performed using the $La_2@C_{80}$ molecule as a prototype lead to the following conclusions:

- The presence of the metal leads alters the internal motion of the La atoms significantly, which instead of rotating almost freely at room temperature in the isolated molecule are constrained to sit near the metal contacts.
- The above-mentioned preference of the La atoms to be close to the metal leads is favored by a net electron charge transfer to the metal.
- The LUMO of the molecule, which is aligned with the La atoms, overlaps extremely well with the metal orbitals, leading to a wide resonance of 1 G_0.
- The relative position of this resonance with respect to the Fermi level is controlled by the charge-transfer process mentioned above: although for gold the peak maximum is placed about 0.8−0.9 eV above the Fermi level depending on the orientation of the [80]fullerene cage with respect to the metal surface, it can be reduced to 0.3 eV either by negatively charging the molecule−gold nanobridge or by using a more electropositive metal such as aluminum.
- Thus, the $La_2@C_{80}$−metal nanobridge may be used as a field-effect transistor. The on−off conductance ratio of such a device also depends on the overlap between the metal states and the HOMO-derived resonances. This, in turn, is governed by the geometry of the metal atoms in contact with the molecule: when tips are used instead of flat surfaces, the on−off ratio can be increased by an order of magnitude, from 25 to 130, due to a sharp decrease of the conductance at the Fermi level.

To summarize, ab initio calculations indicate that the internal movement of La atoms in $La_2@C_{80}$ is hindered when the molecule is sandwiched between two metal electrodes via a charge-transfer process, leading to an electronic nanodevice whose transport properties are highly influenced by the total charge present in it, with large on−off conductance ratios for tip−molecule−tip or tip−molecule−surface geometries of the nanobridge.

Acknowledgment. Financial support from Spanish Ministerio de Educación y Ciencia (MEC) and the European Regional Development Fund through project CTQ2004-06519/BQU, as well as from the Universidad de Alicante (VIGROB-107) is gratefully acknowledged. I thank the Spanish MEC and the Generalitat Valenciana for economic support within the "Ramón y Cajal" program.

References and Notes

(1) Joachim, C.; Gimzevski, J. K.; Aviram, A. *Nature* **2000**, *408*, 541.
(2) Tour, J. M. *Acc. Chem. Res.* **2000**, *33*, 791.
(3) *Nanoelectronics and Information Technology*, 2nd ed.; Waser, R., Ed.; Wiley-VCH: Weinheim, Germany, 2005.
(4) Tour, J. M. *Molecular Electronics. Commercial Insights, Chemistry, Devices, Architecture and Programming*, 1st ed.; World Scientific: Singapore, 2003.
(5) Balzani, V.; Credi, A.; Venturi, M. *Molecular Devices and Machines. A Journey into the Nanoworld*, 1st ed.; Wiley-VCH: Weinheim, Germany, 2004.
(6) Guha, S.; Nakamoto, K. *Coord. Chem. Rev.* **2005**, *249*, 1111−1132.
(7) Kobayashi, S.; Mori, S.; Satoru, I.; Ando, H.; Takenobu, T.; Taguchi, Y.; Fujiwara, A.; Taninaka, A.; Shinohara, H.; Iwasa, Y. *J. Am. Chem. Soc.* **2003**, *125*, 8116−8117.
(8) Kobayashi, K.; Nagase, S.; Akasaka, T. *Chem. Phys. Lett.* **1996**, *261*, 502−506.
(9) Akasaka, T.; Nagase, S.; Kobayashi, K.; Wälchli, M.; Yamamoto, K.; Funasaka, H.; Kako, M.; Hoshino, T.; Erata, T. *Angew. Chem., Int. Ed.* **1997**, *36*, 1643−1645.
(10) Shimotani, H.; Ito, T.; Y., I.; Taninaka, A.; Shinohara, H.; Nishibori, E.; Takata, M.; Sakata, M. *J. Am. Chem. Soc.* **2004**, *126*, 364−369.
(11) Kobayashi, K.; Nagase, S.; Akasaka, T. *Chem. Phys. Lett.* **1995**, *245*, 230−236.
(12) Shinohara, H. *Rep. Prog. Phys.* **2000**, *63*, 843−892.
(13) Kobayashi, K.; Nagase, S.; Maeda, Y.; Wakahara, T.; Akasaka, T. *Chem. Phys. Lett.* **2003**, *374*, 562−566.
(14) Yamada, M.; Nakahodo, T.; Wakahara, T.; Tsuchiya, T.; Maeda, Y.; Akasaka, T.; Kako, M.; Yoza, K.; Horn, E.; Mizorogi, N.; Kobayashi, K.; Nagase, S. *J. Am. Chem. Soc.* **2005**, *127*, 14570−14571.
(15) Yamada, M.; Wakahara, T.; Nakahodo, T.; Tsuchiya, T.; Maeda, Y.; Akasaka, T.; Yoza, K.; Horn, E.; Mizorogi, N.; Nagase, S. *J. Am. Chem. Soc.* **2006**, *128*, 1402−1403.
(16) Frisch, M. J.; Trucks, G. W.; Schlegel, H. B.; Scuseria, G. E.; Robb, M. A.; Cheeseman, J. R.; Montgomery, J. A., Jr.; Vreven, T.; Kudin, K. N.; Burant, J. C.; Millam, J. M.; Iyengar, S. S.; Tomasi, J.; Barone, V.; Mennucci, B.; Cossi, M.; Scalmani, G.; Rega, N.; Petersson, G. A.; Nakatsuji, H.; Hada, M.; Ehara, M.; Toyota, K.; Fukuda, R.; Hasegawa, J.; Ishida, M.; Nakajima, T.; Honda, Y.; Kitao, O.; Nakai, H.; Klene, M.; Li, X.; Knox, J. E.; Hratchian, H. P.; Cross, J. B.; Bakken, V.; Adamo, C.; Jaramillo, J.; Gomperts, R.; Stratmann, R. E.; Yazyev, O.; Austin, A. J.; Cammi, R.; Pomelli, C.; Ochterski, J. W.; Ayala, P. Y.; Morokuma, K.; Voth, G. A.; Salvador, P.; Dannenberg, J. J.; Zakrzewski, V. G.; Dapprich, S.; Daniels, A. D.; Strain, M. C.; Farkas, O.; Malick, D. K.; Rabuck, A. D.; Raghavachari, K.; Foresman, J. B.; Ortiz, J. V.; Cui, Q.; Baboul, A. G.; Clifford, S.; Cioslowski, J.; Stefanov, B. B.; Liu, G.; Liashenko, A.; Piskorz, P.; Komaromi, I.; Martin, R. L.; Fox, D. J.; Keith, T.; Al-Laham, M. A.; Peng, C. Y.; Nanayakkara, A.; Challacombe, M.; Gill, P. M. W.; Johnson, B.; Chen, W.; Wong, M. W.; Gonzalez, C.; Pople, J. A. *Gaussian 03*, revision C.02; Gaussian, Inc.: Wallingford, CT, 2004.
(17) Hohenberg, P.; Kohn, W. *Phys. Rev.* **1964**, *136*, B864−B871.
(18) Kohn, W.; Sham, L. J. *Phys. Rev.* **1965**, *140*, A1133−A1138.
(19) Becke, A. D. *J. Chem. Phys.* **1993**, *98*, 5648−5652.
(20) Stephens, P. J.; Devlin, F. J.; Chablowski, C. F.; Frisch, M. J. *J. Phys. Chem.* **1994**, *98*, 11623−11627.
(21) Dunning, T. H., Jr.; Hay, P. J. Gaussian Basis Sets for Molecular Calculations. In *Modern Theoretical Chemistry: Methods of Electronic Structure Theory*; Schaefer, H. F., III, Ed.; Plenum Publishing Company: New York, 1977; Vol. III.
(22) Hay, P. J.; Wadt, W. R. *J. Chem. Phys.* **1985**, *82*, 270−283.
(23) Roos, R. B.; Powers, J. M.; Atashroo, T.; Ermler, W. C.; LaJohn, L. A.; Christiansen, P. A. *J. Chem. Phys.* **1990**, *93*, 6654−6670.
(24) Palacios, J. J.; Pérez-Jiménez, A. J.; Jacob, D.; Louis, E.; San-Fabián, E.; Vergés, J. A. http://www.guirisystems.com/alacant.
(25) Datta, S. *Electronic Transport in Mesoscopic Systems*; Cambridge University Press: Cambridge, 1995.
(26) Palacios, J. J.; Pérez-Jiménez, A. J.; Louis, E.; Vergés, J. A. *Phys. Rev. B* **2001**, *64*, 115411.
(27) Palacios, J. J.; Pérez-Jiménez, A. J.; Louis, E.; SanFabián, E.; Vergés, J. A. *Phys. Rev. B* **2002**, *66*, 035322.
(28) Louis, E.; Vergés, J. A.; Palacios, J. J.; Pérez-Jiménez, A. J.; SanFabián, E. *Phys. Rev. B* **2003**, *67*, 155321.
(29) Palacios, J. J.; Pérez-Jiménez, A. J.; Louis, E.; SanFabián, E.; Vergés, J. A.; García, Y. Molecular electronics with Gaussian98/03. In *Computational Chemistry: Reviews of Current Trends*; Leszczynski, J., Ed.; World Scientific: Singapore, 2005; Vol. 9.
(30) Nishibori, E.; Takata, M.; Sakata, M.; Taninaka, A.; Shinohara, H. *Angew. Chem., Int. Ed.* **2001**, *40*, 2998−2999.
(31) Kubozono, Y.; Takabayashi, Y.; Kashino, Y.; Kondo, M.; Wakahara, T.; Akasaka, T.; Kobayashi, K.; Nagase, S.; Emura, S.; Yamamoto, K. *Chem. Phys. Lett.* **2001**, *335*, 163−169.
(32) Ton-That, C.; Shard, A. G.; Egger, S.; Dhanak, V. R.; Taninaka, A.; Shinohara, H.; Welland, M. E. *Phys. Rev. B* **2003**, *68*, 045424.
(33) Fujitsuka, M.; Ito, O.; Kobayashi, K.; Nagase, S.; Yamamoto, K.; Kato, T.; Wakahara, T.; Akasaka, T. *Chem. Lett.* **2000**, 902−903.
(34) Suzuki, T.; Maruyama, Y.; Kato, T.; Kikuchi, K.; Nakao, Y.; Achiba, Y.; Kobayashi, K.; Nagase, S. *Angew. Chem., Int. Ed.* **1995**, *34*, 1094−1096.
(35) Taninaka, A.; Shino, K.; Sugai, T.; Heike, S.; Terada, Y.; Hashizume, T.; Shinohara, H. *Nano. Lett.* **2003**, *3*, 337−341.
(36) Park, H.; Park, J.; Lim, A. K. L.; Anderson, E. H.; Alivisatos, A. P.; McEuen, P. L. *Nature* **2000**, *407*, 57−60.
(37) Park, J.; Pasupathy, A.; Goldsmith, J. I.; Chang, C.; Yaish, Y.; Petta, J. R.; Rinkoski, M.; Sethna, J. P.; Abruna, H.; McEuen, P. L.; Ralph, D. C. *Nature* **2002**, *417*, 722−725.
(38) Liang, W.; Shores, M. P.; Bockrath, M.; Long, J. R.; Park, H. *Nature* **2002**, *417*, 725−729.
(39) Lang, N. D. *Phys. Rev. B* **2001**, *64*, 235121.